Research Highlights

Microbeam High-resolution Diffraction and X-ray Standing Wave Techniques at CHESS

A. Kazimirov[1], D. H. Bilderback[1], R. Huang[1] and A. Sirenko[2]

[1]*Cornell High Energy Synchrotron Source, Cornell University*
[2]*New Jersey Institute of Technology, University Heights, Newark, NJ 07102-1982*

Introduction

High angular resolution X-ray diffraction (HRXRD) and scattering techniques in their different modifications and experimental geometries [1] emerged in 1980's based on progress in development of X-ray dynamical diffraction theory and driven by the needs of the fast growing semiconductor industry. High-resolution diffractometry became one of the major characterization tools for semiconductor technology providing important information about strain, composition, mosaic structure and defect density in thin surface layers. Nowadays, modern technology successfully produces solid state structures with dimensions ranging from several nanometers (quantum wires and dots) to several microns (optoelectronic devices, MEMS). For characterization of these structures, X-ray techniques combining both high spatial and high angular resolution have to be developed.

Remarkable progress in X-ray focusing during recent years has made it possible to produce sub-micron size beams using a variety of different focusing optics [2]. However, any focusing optic creates a convergent X-ray beam making it useless for high angular resolution experiments. There are several approaches to overcome this problem. The first one is based on using a pinhole [3]. The pinhole, however, significantly deteriorates the angular resolution due to diffraction effects, and the intensity of the microbeam is limited by the flux density of the incident beam. A highly collimated monochromatic X-ray microbeam of 7 μm by 5 μm was produced by collimating an undulator beam by slits and compressing it further with multi-crystal optics [4]. However, the low intensity of this beam as a result of the two-dimensional collimation makes it problematic for use in intensity limited experiments such as reciprocal space mapping or X-ray Standing Waves (XSW). The microbeam XSW technique has been recently demonstrated based on one-dimensional vertical focusing of the undulator beam [5]. In our recent experiments at CHESS we proposed and successfully tested a new approach based on two-dimensional focusing and post-focusing collimating optics [6].

Experiment: HRXRD

The experimental setup used at the CHESS D1 bending magnet beamline is shown in Figure 1a. The energy of the X-ray beam was tuned to 12.5 keV by using a double-crystal multilayer monochromator with a band pass of 1.1 %. A one-bounce imaging capillary [7] with a working distance of 30 mm and a gain of 75 produced an X-ray beam with a circular size of 10 μm FWHM and a divergence of 4 mrad. A miniature Si(400) two-bounce channel-cut crystal with a channel width of 0.5 mm was designed for this experiment and inserted between the tip of the capillary and the focal spot. A close-up view photo of the setup is shown in Figure 1b.

The X-ray beam in front of the channel-cut crystal has a wide energy spread from the upstream multilayer optics and a wide angular spread created by the focusing capillary. To characterize the ultimate angular resolution of the optics, the (004) rocking curve from the standard Si(001) wafer was measured by rocking the Si(004) channel cut crystal in the 4 mrad convergent beam from the capillary. A rocking curve width of 14 μrad was observed in good agreement with the theory (inset in Figure 1a) demonstrating the excellent angular resolution of the setup.

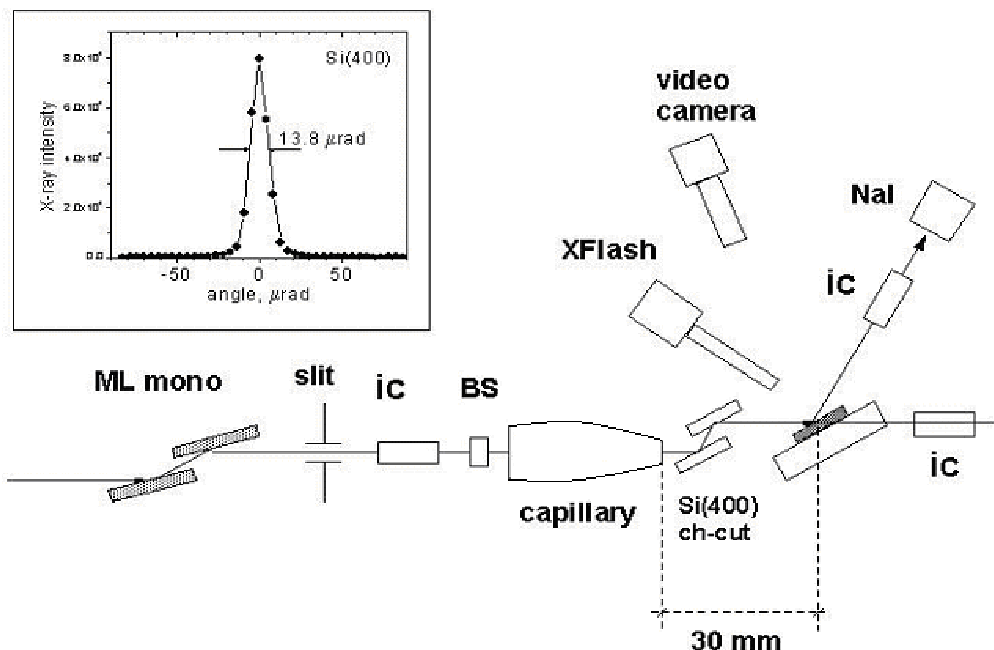

Fig 1: (Top) Experimental setup for the microbeam high resolution diffraction and x-ray standing wave measurements at CHESS based on a collimating miniature Si(400) channel cut crystal and a one-bounce imaging capillary with a working distance of 30 mm and a beam size at the focal spot of 10 µm. The beam stop BS is blocking the through beam. The energy dispersive XFlash detector is used to monitor fluorescence yield. The sample was mounted on a computer controlled XY piezo stage (spatial resolution of 2 nm) and assembled on a one-circle goniometer with a horizontal rotation axis. The inset shows the Si(400) instrumentation rocking curve. (Right) Photo of the setup showing focusing capillary, miniature channel cut crystal, sample with structure pattern and Xflash energy dispersive detector.

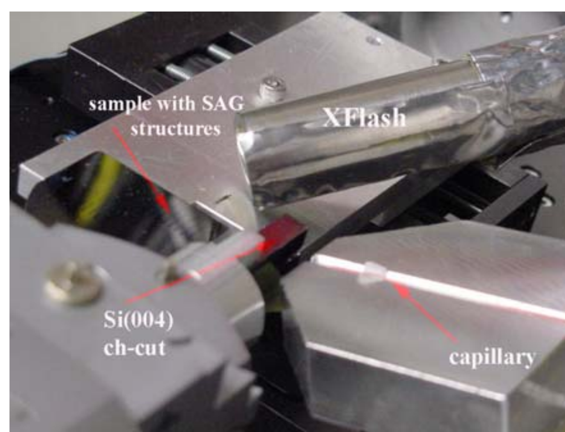

The microbeam was used for HRXRD and XSW characterization of quaternary $In_{1-x}Ga_xAs_yP_{1-y}$ semiconductor layers selectively grown by metal organic vapor phase epitaxy (MOVPE) on stripe regions of an InP(001) substrate surrounded by a pair of SiO_2 dielectric mask stripes. Selective area growth (SAG) became recently one of the most important technological methods for production of monolithically integrated III-V semiconductor structures such as electro absorption modulated lasers, waveguides, amplifiers, mixers, and other optoelectronic telecommunication devices. By varying the geometry of the oxide pattern (Figure 2), epitaxial layers with different physical properties can be grown simultaneously on the same InP wafer [8].

A high spatial resolution study of both thickness and composition variations in the grown layers is crucial for understanding and modeling of the SAG process and for optimization of new optoelectronic devices. In our previous experiment [9], we combined microbeam X-ray fluorescence analysis based on a multibounce condensing capillary with a beam size of 1 µm and the micro-photoluminescence technique to measure both thickness and composition variations in ternary and quaternary SAG layers.

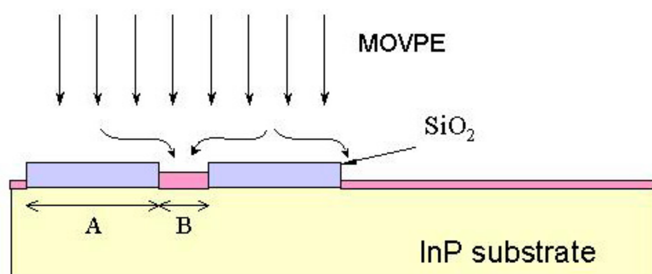

Fig 2: Illustration of selective area growth based on metal organic vapor phase epitaxy (MOVPE). The molecules of the growing crystalline material migrate on SiO_2 surface until they reach semiconductor surface where they are built into the lattice of the growing film. The composition and the thickness of the film growing between two oxide masks can be controlled by the geometry of the oxide pattern, i.e. the width of the oxide mask A and the size of the gap B. This way, growth of layers with different band structure can be performed simultaneously.

In this work we studied $In_{1-x}Ga_xAs_yP_{1-y}$ layers with parameters in the open regions of the wafer of x=0.32, y=0.6, and a thickness of 0.14 μm grown by the SAG technique in the opening between two 600 μm-long SiO_2 mask stripes. The width of the oxide stripe **A** varied from 10 to 140 μm and the opening between two oxide masks, **B**, varied from 15 to 80 μm. The sample was mounted on a computer controlled XY piezo stage with a spatial resolution of 2 nm assembled on a one-circle goniometer with a horizontal rotation axis. The beam was positioned between the oxide masks by monitoring the As-K_α and Ga-K_α fluorescence. All diffraction scans were performed by scanning the Si(400) collimating channel-cut crystal in the focused beam produced by the capillary.

Two series of the HRXRD curves were measured, one for structures with constant **A** = 140 μm and **B** changing from 80 to 20 μm and the second for **B** = 30 μm and **A** varying from 140 μm to 45 μm. The strain data deduced from the diffraction curves is in excellent agreement with the results based on our non-diffraction analysis [9].

In both series of measurements we observed a change of the sign of the strain at certain **B (A)** values. The HRXRD curves and the strain data for **B** = 30 μm and different widths of the oxide mask are shown in Figure 3. In the regions where the strain changes sign the diffraction peaks from the substrate and the film overlap making accurate strain measurements problematic. We demonstrate that for these structures microbeam XSW technique can be used for more precise measurements.

Experiment: XSW

The sensitivity of the XSW technique to the lattice constant mismatch depends on the thickness of the film t_f and the magnitude of the fluorescent yield t_{yi}. When the fluorescence is collected from the entire thickness of the film ($t_{yi} = t_f$) the standing wave loses its "coherence" with the atomic lattice of the film at the mismatch of $\Delta d/d > d/t_f$ and the XSW response curve becomes $1+R(\theta)$, ($R(\theta)$ is the reflectivity curve) and not sensitive to changes in $\Delta d/d$. In the range of $\Delta d/d < d/t_f$, where the X-ray diffraction curve is not sensitive to $\Delta d/d$ due to the overlap of the weak film peak with the strong substrate peak, the XSW method can be used for accurate strain measurements [10,11].

Two adjacent structures with **B** = 30 μm and **A** = 60 μm and 70 μm were chosen for further study where the diffraction curves indicated an opposite sign of strain. The fluorescent spectrum from the sample was collected for each angular point of the rocking curve while performing multiple angular scans through the Bragg (004) peak. The XSW scans were performed by scanning the Si(400) channel cut crystal. The fluorescence yield and X-ray curves were normalized by the angular distribution of the incident beam intensity after the channel cut. Enhancement in the As-K fluorescence yield (Figure 4, right panel) from the film with **A** = 70 μm is clearly observed due to the shift of As atoms into the region of the stronger standing wave field indicating the presence of positive ($\Delta d/d>0$) strain in the film. The opposite effect for the structure with **A** = 60 μm indicates negative strain.

The experimental XSW data were analyzed by a computer program based on the dynamical theory of X-ray diffraction and XSW in multilayered crystal systems [12]. The In-L fluorescence originates mainly from the InP substrate. The fit yielded a very reasonable value of the static Debye-Waller factor $e^{-Wst} = 0.96$ ($e^{-Wst} = 1.0$ for ideal lattice). The excellent fit to the experimental data indicated well-controlled standing wave behavior and validated the proposed experimental scheme. Fitting the As-K fluorescence yield from the SAG layers we assumed fixed layer thickness values of 0.231 μm for **A** = 70 μm and 0.217 μm for **A** = 60 μm determined in [9]. The strain data determined by the XSW measurements,
$\Delta d/d = +3.3 \times 10^{-4}$ for A = 70 μm and $\Delta d/d = -1.1 \times 10^{-4}$ for A = 60 μm, are shown by filled circles in the inset on Figure 3. The dashed curve in Figure 4 shows the As-K fluorescence yield from the layer with zero strain demonstrating the sensitivity of the XSW method.

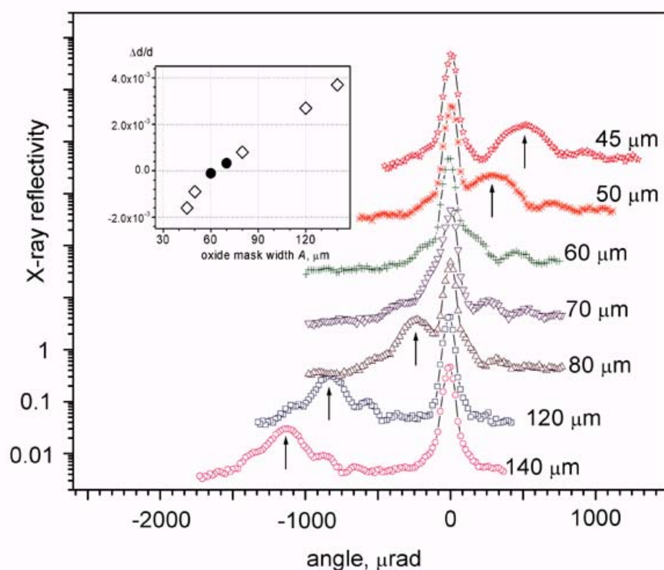

Fig 3: Experimental HRXRD curves from the quaternary $In_{1-x}Ga_xAs_yP_{1-y}$ SAG layers grown in a 30 μm wide (**B**) area between two 600 μm long SiO_2 mask stripes measured for different values of the SiO_2 mask width **A**. The positions of the SAG layer peaks are indicated. The scans were performed by scanning the channel-cut crystal in the convergent focused beam. The strain data determined from the diffraction (open diamonds) and the XSW (solid circles) experiments is shown in the upper inset.

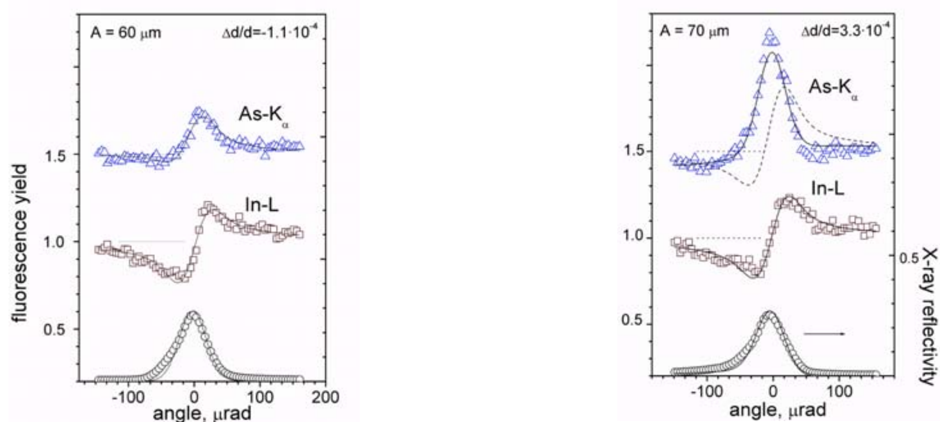

Fig 4: Experimental x-ray rocking curve and XSW As-K and In-L fluorescence yield from the $In_{1-x}Ga_xAs_yP_{1-y}$ SAG structure grown in a 30 μm wide area between 60 μm (left) and 70 μm (right) wide oxide masks. The best fit (solid lines) for the As-K yield curve corresponds to the strain $\Delta d/d = -1.1\times10^{-4}$ and $+3.28\times10^{-4}$ measured from the structure with **A**=60 μm and **A**=70 μm, correspondingly. The dotted horizontal lines show off-Bragg normalized yield. For comparison, the dash curve shows As-K fluorescence yield from the structure with zero strain

Discussion and outlook

Liouville's theorem (preservation of the phase space) imposes limitations on the minimum beam size for diffraction-limited focusing optics: the more narrow the acceptance angle of the collimating crystal the larger the minimum size. Using the Airy formula as a guide [13] we can estimate that the minimum pbtainable beam size in the diffraction plane for 12.5 keV X-rays varies from about 1 μm for Ge(111) to 6 μm for Si(400) collimating crystals. The beam size perpendicular to the diffraction plane should not be affected. We measured the size of the beam in both vertical (diffraction) and horizontal planes with and without the collimating crystal by scanning the edge of the epitaxial film and measuring the As-K_α and Ga-K_α fluorescence yield from the film. We observed a beam size of 10±1 μm (FWHM) in both directions. Thus, within our experimental error-bars, for the 10 μm beam used in our experiment we did not see any significant broadening of the beam by the collimating crystal in the diffraction plane.

Post-focusing collimating crystals can be designed individually for the needs of a particular experiment and the type of the crystal under study to achieve maximum flux on the sample and/or minimum size of the beam when diffraction-limited optics situations are encountered. The possibility to perform scans by scanning a channel-cut crystal in the converging focused beam significantly simplifies the experiment. The experimental approach developed in this paper has potential application for future analysis of micron- and sub-micron size microelectronic device structures. It can also be applied to other microbeam techniques that require high angular resolution such as reciprocal space mapping, reflectometry, and ultra-small angle scattering using Fresnel zone plates, refractive lenses, KB mirrors, and capillaries, to create the microbeams.

References:

[1] D.K. Bowen and B.K. Tanner, *"High Resolution X-ray Diffractometry and Topography"*, Taylor & Francis (1998); V. Holý, U. Pietsch, and T. Baumbach, *"High-Resolution X-Ray Scattering from Thin Films and Multilayers"*, Springer Tracts in Modern Physics, **149**, (1999).
[2] C. Riekel, Rep. Prog. Phys. **63**, 233-262 (2000).
[3] Z.-H. Cai, W. Rodrigues, P. Ilinski, D. Legnini, B. Lai, W. Yun, E.D. Isaacs, K.E. Lutterodt, J. Grenko, R. Glew, S. Sputz, J. Vandenberg, R. People, M.A. Alam, M. Hybertsen, and L.J.P. Ketelsen, Appl. Phys. Lett., **75**, 100 (1999).
[4] Y. Tsusaka, K. Yokoyama, S. Takeda, M. Urakawa, Y. Kagoshima, J. Matsui, S. Kimura, H. Kimura, K. Kobayashi, and K. Izumi, Jpn. J. Appl. Phys. **39**, L635 (2000).
[5] M. Drakopoulas, J. Zegenhagen, A. Snigirev, I. Snigireva, M. Hauser, K. Eberl, V., Aristov, L. Shabelnikov, and V. Yunkin, Appl. Phys. Lett. **81**, 2279 (2002).
[6] A. Kazimirov, D. H. Bilderback, R. Huang, A. Sirenko, A. Ougazzaden, Journal of Physics D: Applied Physics, Rapid Communications, **37**, L9-L12, (2004).
[7] D. H. Bilderback and E. Fontes, AIP Conference Proceedings, **417**, 147 (1997).
[8] S. Sudo, K. Kudo, K. Mori, and T. Sasaki, Conference Proceedings of the International Conference on InP and Related Materials, IPRM' 2001, p. 390.
[9] A. A. Sirenko, C. L. Reynolds, L. J. Peticolas, A. Ougazzaden, A. Kazimirov, R. Huang, E. Fontes, and D. Bilderback, J. Cryst. Growth **253**, 38 (2003).
[10] A. Yu. Kazimirov, M.V. Kovalchuk, and V.G. Kohn, Sov. Tech. Phys. Lett. **14**, 587 (1988).
[11] A. Kazimirov, J. Zegenhagen, M. Cardona, Science **282**, 930 (1998).
[12] V.G. Kohn, Phys. Stat. Sol. (b) **231**, 132 (2002).
[13] D. Attwood, *"Soft X-Rays and Extreme Ultraviolet Radiation: Principles and Applications"*, Cambridge University Press, (1999).